Chemical Engineering Journal 350 (2018) 233–239

Contents lists available at ScienceDirect

Chemical Engineering Journal

journal homepage: www.elsevier.com/locate/cej

Local mass-transfer study in a decaying swirling flow electrochemical reactor under single-phase and two-phase (gas-liquid) flow

C.C. Contigiani, O. González Pérez, J.M. Bisang*

Universidad Nacional del Litoral, CONICET, Programa de Electroquímica Aplicada e Ingeniería Electroquímica (PRELINE), Facultad de Ingeniería Química, Santiago del Estero 2829, S3000AOM Santa Fe, Argentina

HIGHLIGHTS

- The swirling flow improves the mass-transfer conditions in a reactor.
- The swirling flow becomes more uniform the mass-transfer distribution.
- The gas phase has scarce influence on the mass-transfer performance.

ARTICLE INFO

Keywords:
Electrochemical reactor
Mass-transfer
Swirling flow
Tangential inlet

ABSTRACT

Mass transfer was studied at the external electrode of a cylindrical electrochemical reactor with decaying swirling flow using a single phase electrolyte and also a dispersion of a gas phase in the solution. The local mass-transfer coefficients were measured with a segmented cathode using the reduction of ferricyanide as test reaction. Two strategies were used to introduce the gas phase. In the first case the gas was fed by three holes symmetrically drilled at the bottom of the central anode tube and in the second one by means of a tee fitting at the reactor inlet. The best performance was obtained with the single phase electrolyte giving 0.78 as the exponent of the Reynolds number and the mass-transfer distribution along the reactor length is more uniform than that reported for a parallel plate electrochemical reactor under laminar flow conditions. The mass-transfer enhancement factor related to an annular duct with axial developing flow ranges from 8 to 11. This high value is the consequence of two factors: (i) the intensive forced convection produced by the swirling flow at the outer electrode and (ii) the sudden expansion of the flow at the entrance due to the small tangential inlet. The fed of a gas phase in the reactor has scarce influence on the mass-transfer performance. A comparison of mass-transfer results with previous studies is made.

1. Introduction

The enhancement of the space time yield in process equipment is of vital importance in order to increase its performance. Two strategies can be used to improve the space time yield of electrochemical reactors with reactions influenced by mass-transfer. The first is the increase of the specific surface area of the electrode arising three-dimensional electrodes. The second one is the enhancement of the mass-transfer conditions in the reactor by modification of its hydrodynamics. Based on the last concept many techniques have been proposed, being the use of swirling flow a promising one. These equipments present as additional advantages: simple constructive features, absence of moving parts and easy to recover the products. In a pioneer work Cedrone [1] proposed a reactor with tangential solution nozzles, located at the bottom of a cylindrical reactor, in order to improve the mass-transfer for silver deposition onto a external cathode. Along the axial length, the solution continues to swirl and climbs in an ascending helix in the interelectrode gap formed by a concentric tube, working as anode. At the top of the reactor the fluid is deflected to the internal part of the anode where it falls into a filter sock suspended within the anodic tube and it runs downward into a sump tank, being again recirculated. Other application of the concept of helical flow was reported by Walsh and Wilson [2] for the removal of gold from spent metal finishing process liquors by means of the “Metelec Concentric Cylindrical Cell”, which incorporates a cylindrical foil cathode concentrically arranged around an inner anode. The inlet and outlet manifolds were tangentially positioned near the bottom and top of the cell, respectively. However, the concept of swirling flow was scarcely explored in electrochemical

* Corresponding author.
E-mail address: jbisang@fiq.unl.edu.ar (J.M. Bisang).

https://doi.org/10.1016/j.cej.2018.05.181
Received 2 February 2018; Received in revised form 28 May 2018; Accepted 30 May 2018
Available online 31 May 2018
1385-8947/

reactors for effluents treatments from dilute solutions, where the achievement of good mass-transfer conditions is a very important goal. Wang [3,4] proposed, for the electrowinning, electrorefining or recovery of metals, the EMEW cell (EMEW Clean Technology, Vancouver, BC, Canada), which consists of a pair of concentric tubes, the inner being an iridium/ruthenium-coated titanium anode and the outer being a rolled stainless-steel sheet cathode held by a polyvinyl chloride outer body. At both ends of the cell are plastic closure caps with liquor inlet and outlet ports.

Likewise, this rotary type of liquid flow causes a reduction in pressure in its central axial part. Then, a gas phase can be introduced to the reduced pressure area. This concept is described as a procedure for the generation of a gas-liquid dispersion with the formation of microbubbles [5], which can be recognised as an interesting proposal for the electrochemical processing of gaseous reagents.

The foregoing industrial applications were developed simultaneously with studies of mass-transfer in these systems, which are under a special hydrodynamic condition frequently called helical or swirl flow. This flow may be classified into two different types according to the method used to achieve the rotation movement: continuous swirl and decayed or damped swirl. In the first type, the swirling motion persists and maintains its characteristics over the entire length of the tube or annular space, while in the second type, the swirl is generated at the inlet section and decays freely along the flow path and its properties vary with axial distance from the entrance. Continuous swirl is usually achieved by inserting twisted tapes, spiral fins or coiled wires of varying pitch, helix angle and wire diameter, along the entire length of the tube. Decaying swirl may be induced by tangential inlet slots or tubes, tangential vanes, short lengths of helical inserts, and rotating cylinders or propellers. The second type is preferred because of its simple design and easy maintenance, due to the absence of inserts, and also by a lower pressure drop in the equipment. Shoukry and Shemilt [6] reported results of mass-transfer in turbulent decaying swirl flow in an annulus. Enhancement of the global mass transfer coefficient of up to 320% was obtained, in comparison with the value for developed axial flow. Legentilhomme and Legrand [7–9] studied the mass-transfer between a liquid and the inner cylinder of an annular gap under decaying swirling flows and an enhancement factor of the global mass-transfer coefficient up to 4 was reported. de Sa et al. [10] corroborated the improvement of the global mass-transfer coefficients by a decaying swirling flow. Yapici et al. [11–13] reported a study of the local mass-transfer behaviour, measured with microelectrodes, in decaying annular swirl flow produced by axial vane-type generators. The mass-transfer coefficients decay towards the value for fully developed flow as the axial distance increases, but, even at 50 equivalent diameters downstream, the effect of swirl is still evident. Lefèbvre et al. [14] corroborated that the mass-transfer coefficient for the outer wall is higher than that for the inner rod. The comparison with previous studies allowed concluding that the use of single tangential entries, to generate the swirl flow, enhances the mass-transfer coefficient due to the higher swirl intensity. In a further contribution, Yapici et al. [15] studied the local mass-transfer distribution in decaying swirl flow in a circular pipe.

The previous studies on mass-transfer in decaying swirl flow do not provide any detailed information on the local mass-transfer distribution for reactors with cylindrical concentric electrodes. This paper describes the results of experimental work on local mass-transfer measurement in decaying annular swirl flow using an electrochemical technique involving a segmented electrode in a home-made reactor. Both, single phase and biphasic system, gas-liquid, were studied.

2. Material and methods

The reactor, shown schematically in Fig. 1, was made of two parallelepiped blocks of acrylic material, 80 mm side and 149 mm length, which were assembled by a threaded joint with an O'ring seal 1 mm thick. In both blocks, it was machined a cylindrical cavity of 42 mm

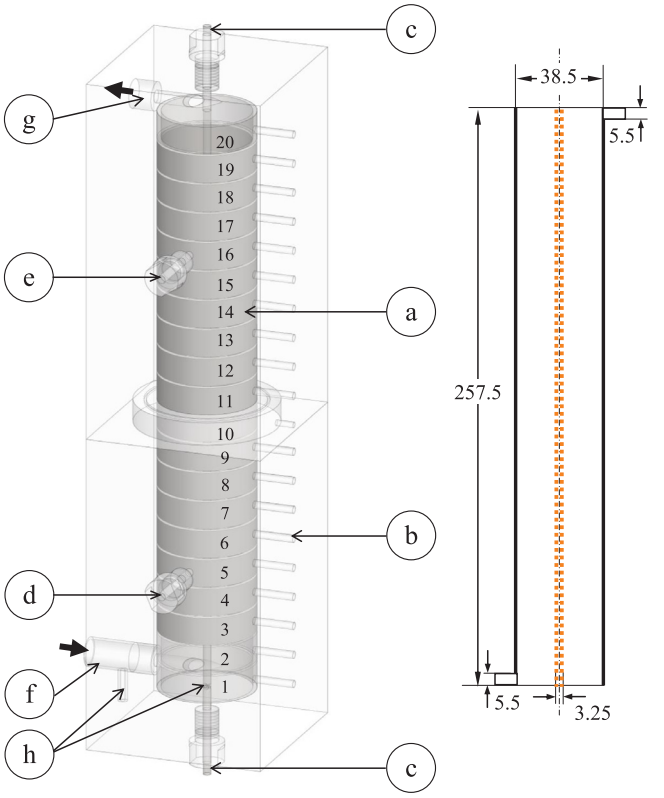

Fig. 1. Schematic representation of the decaying swirling flow electrochemical reactor. (a) Segmented cathode; (b) electrical connections to calibrated resistors; (c) electrical connection to anode; (d) Haber-Luggin capillary for cathodic potential control; (e) second Haber-Luggin capillary for measurement of the cathodic potential; (f) tangential electrolyte inlet; (g) tangential electrolyte outlet; (h) nitrogen feeder for biphasic system. The numbers indicate the position of the segments and the arrows the flow of the electrolyte. Right hand side: thick full line: cathode; thick dotted line: anode. Internal dimensions of the reactor in mm.

diameter in whose internal wall the segmented cathode was arranged, made of 20 segments of 316 stainless steel, 38.5 mm internal diameter and 12 mm length. The segments were insulated from one another by a polyamide ring of approximately 1 mm thick. Thus, the total length of the segmented cathode was 257.5 mm and its surface was polished with emery paper 2500 grade. The insulating insertions between segments disturb the concentration profiles at the electrode surface [16] altering the mass-transfer behaviour. However, in a previous work [17] it was demonstrated using computational fluid dynamics that the maximum error in the measurement of the mass-transfer coefficient, as a result of the use of a segmented electrode with level separators, may be in the order of 14%, which is an acceptable value for this type of experiments. However, the presence of recessed insulating insertions between segments additionally produces a turbulence promotion action generating a greater increase in the mass-transfer coefficient [18].

The electrical contact to the external electrode was made by a screw through the acrylic wall pressing the backside of each segment. Calibrated resistors, 0.025 Ω resistance, join the screws of each segment and the cathodic current feeder, which was electrically connected at both ends. By measuring the ohmic drop in the resistors, it was possible to determine the axial current distribution and to calculate the local mass-transfer coefficient at each segment. The effect of the calibrated resistors on the current distribution can be neglected due to the small value of their ohmic drop, lower than 5 mV, in comparison with the other terms of the voltage balance in the reactor. The data acquisition was performed using a computer controlled home-made analogue multiplexer and five independent data sets were obtained for each

controlled potential. During an experiment all the segments were connected to the cathodic current feeder, unless otherwise is stated. The cathodic potential was controlled against a saturated calomel electrode, SCE, connected to a Haber-Luggin capillary positioned at 58 mm from the reactor bottom, in the central part of the fifth segment. The capillary was introduced from the backside of the segment through a hole machined in it and in the acrylic wall. The cathodic potential was also measured in the sixteenth segment, by means of a second Haber-Luggin capillary placed at 58 mm from the reactor top, in order to corroborate that the upper part of the cathode works under limiting current conditions. The experiments were carried out potentiostatically at potentials ranging from −0.7 V to −1.1 V, verifying that a limiting current was achieved. The anode was made of a 316 stainless steel tube, 3.25 mm external diameter, placed in the central axis of the equipment from the top to the bottom. This arrangement becomes uniform the primary potential distribution inside the reactor. To avoid the anodic dissolution of the stainless steel tube, the anode was electroplated with nickel from a conventional Watts-type bath [19] to get a nickel thickness of 50 μm and it was electrically connected at both ends in order to ensure isopotentiality of the anodic metal phase. The scheme on the right hand side of Fig. 1 summarises the internal dimensions of the reactor. The annular thickness or interelectrode gap was 17.6 mm and the electrolyte volume inside the reactor was 0.2976 dm^3. The volume of solution in each run amounted to capacity 4 dm^3. The solution was fed from a reservoir to the reactor by means of a tangential inlet at the bottom and the outlet was made with a tangential port at the top part of the equipment, both ports of 5.5 mm diameter. The small size of the ports, respect to the interelectrode gap, was chosen in order to obtain a large tangential velocity at the reactor inlet, generating an expansion swirl flow with an expansion factor of 3.2 which improves the mass-transfer behaviour [8]. The initial swirl intensity was 48.7 [7].

The reactor was made part of a flow circuit system consisting of a pump, a flow meter, a reservoir and connections to maintain the temperature at the preset value, 30 °C. The inlet volumetric flow rate, Q, was changed in the range of 2–10 dm^3/min.

The test reaction for the mass-transfer studies was the electrochemical reduction of ferricyanide with $[K_3Fe(CN)_6] \cong 0.01$ mol/dm^3 and $[K_4Fe(CN)_6] \cong 0.15$ mol/dm^3 in 1.75 mol/dm^3 of K_2CO_3 as supporting electrolyte, while the reverse reaction occurred at the anode. Nitrogen was bubbled in the reservoir for 1 h prior to the experiment with the aim of remove the dissolved oxygen. A large difference in concentration between ferricyanide and ferrocyanide was chosen in order to avoid oxygen evolution as a secondary reaction at the anode due to its smaller surface area. The high concentration of supporting electrolyte was adopted to diminish the oxygen solubility in the electrolyte [20]. Thus, the current for the reduction of the residual oxygen after bubbling nitrogen is negligible in comparison with the reduction current of ferricyanide from this dilute solution. Table 1 summarizes the composition and physicochemical properties of the electrolyte [21]. Samples of the solution were taken from the reservoir after each experiment and the ferricyanide concentration was spectrophotometrically determined using 10 mm quartz absorption cells and the supporting electrolyte was used as blank. The measurements were performed at a wavelength of 420 nm, where it is possible to determine the ferricyanide concentration without any interference of ferrocyanide.

Table 1
Physicochemical properties of the ferricyanide/ferrocyanide solution.

Composition	$[K_3Fe(CN)_6] = 1 \times 10^{-2}$ mol/dm^3 $[K_4Fe(CN)_6] = 0.15$ mol/dm^3 $[K_2CO_3] = 1.75$ mol/dm^3
ν (m^2/s)	1.52×10^{-6}
D (m^2/s)	5.3×10^{-10}
Sc	2868

In the experiments using a biphasic system, nitrogen was fed at the reactor bottom employing two strategies. In the first case, the gas phase was introduced through the anode tube by means of three holes, 1 mm diameter, drilled symmetrically at 120° from one another. In the second one, nitrogen was supplied together with the electrolyte by a tee fitting at the reactor inlet. The gas volumetric flow rate, Q_g, was changed in the range of 0.6–2 dm^3/min, under ambient conditions.

The local mass-transfer coefficient, $k_{m,y}$, was calculated from the limiting current at each segment, $I_{lim,i}$, and the reactant bulk concentration, c, using the following equation [22]:

$$k_{m,y} = \frac{I_{lim,i}}{\nu_e F A_i c} \quad (1)$$

where A_i is the surface area of the i-th segment at the axial position y, ν_e is the number of electrons interchanged and F is the Faraday constant. The global mass-transfer coefficient, $k_{m,\ global}$, was computed in accordance to:

$$k_{m,\ global} = \frac{\sum_{i=1}^{20} k_{m,y} A_i}{\sum_{i=1}^{20} A_i} \quad (2)$$

3. Results and discussion

3.1. Mass-transfer studies in the single-phase system

Fig. 2 displays polarization curves, for a volumetric flow rate of 4 dm^3/min, of each segment in the reactor being the other segments disconnected. The segments are numbered from bottom (1) to top (20), as shown in Fig. 1. Fig. 2 Part (a) reveals that the polarization curve for the fifth segment, where the Haber-Luggin tip was placed, presents limiting current conditions for potentials ranging from −0.6 V to −1.2 V corroborating previously reported data with the use of a rotating disc electrode changing the rotation speed [21]. At potentials more negative than −1.2 V an abrupt increase in current is observed attributable to hydrogen evolution. The other segments show a similar kinetic behaviour but the limiting current region and the onset of hydrogen evolution is delayed to more negative potentials as a consequence of the ohmic drop between the Haber-Luggin tip and the segment surface. However, in all cases a well defined limiting current density is observed in a broad potential-span of approximately 0.5 V. Fig. 2 Part (a) also shows that the limiting current density decreases at the first half of the reactor being the decay more marked in the three first segments, which can be attributed to the influence of flow expansion at the reactor inlet. Considering that in the present case the abrupt expansion is not axisymmetric, it can be inferred that the separation, reattachment, redevelopment experienced by the flow and its influence on the mass-transfer behaviour is strongly dependent on the size of the interelectrode gap. Fig. 2 Part (b) reports that the diminution of the limiting current density is less pronounced in the second part of the reactor. This behaviour can be explained taking into account that the swirling flow is dampened along the reactor length. However, in the last two segments the limiting current density increases again as a consequence of the influence of the tangential outlet port on the hydrodynamics.

Fig. 3 reports on typical curves of the local mass-transfer coefficient as a function of the axial position in the reactor for different values of the volumetric flow rate, Q, being all the segments simultaneously connected. The symbols at each potential correspond to the results of five independent measurements, obtaining a good reproducibility between them. Likewise, the close agreement between the data at different potentials corroborates that limiting current conditions were achieved at each segment. For all volumetric flow rates a range of potentials was detected where the reaction takes place under limiting current conditions. This potential range is lower as the volumetric flow rate is increased as a consequence of the potential distribution along the

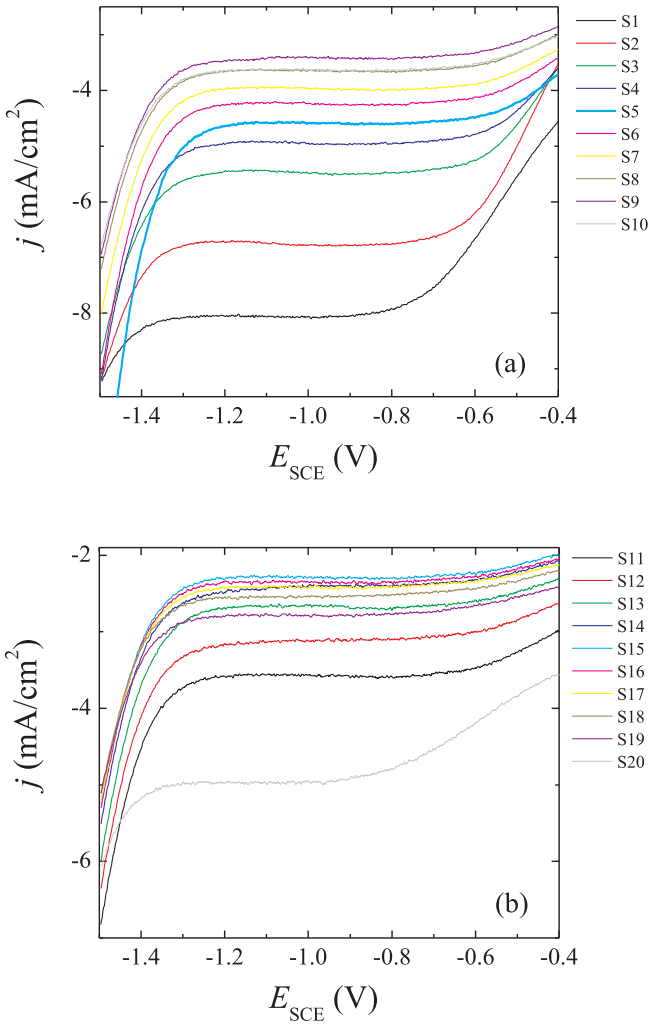

Fig. 2. Polarization curves at each segment being the other segments disconnected. Part (a): segments 1–10. Part (b): segments 11–20. Si: segment at the i-th position, being 1 the bottom one as it is shown in Fig. 1. Ferricyanide reduction from a solution with $[K_3Fe(CN)_6] = 0.009\ mol\ dm^{-3}$ and $[K_4Fe(CN)_6] \cong 0.15\ mol\ dm^{-3}$ in $1.75\ mol\ dm^{-3}$ of K_2CO_3 as supporting electrolyte. $Q = 4\ dm^3/min$. Scan rate: $2\ mV\ s^{-1}$.

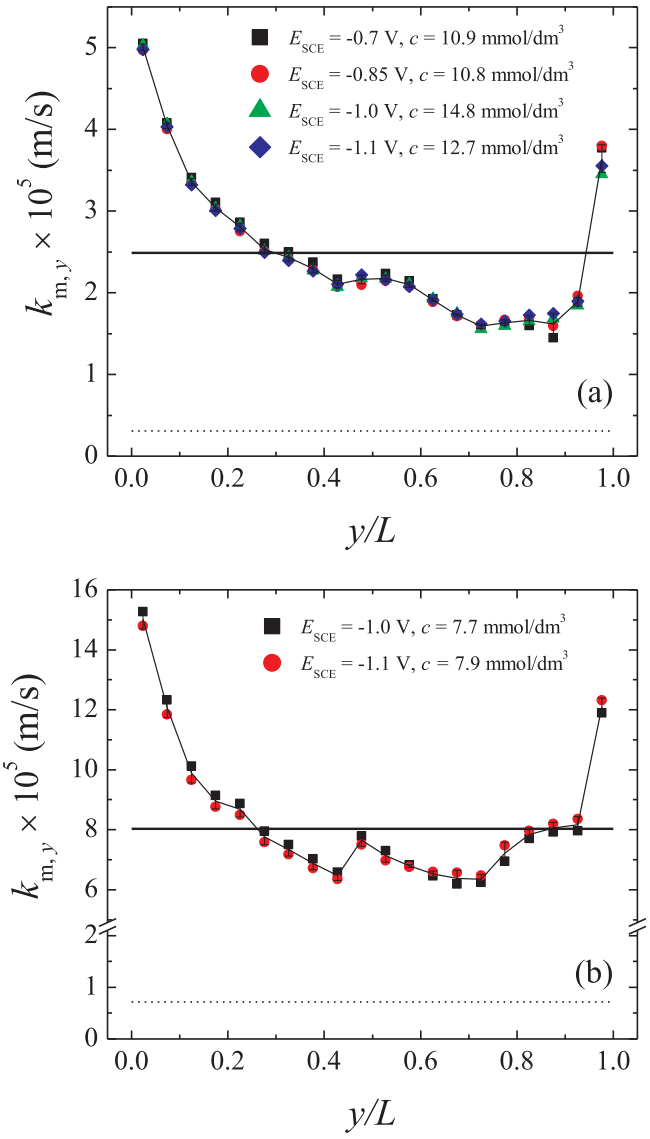

Fig. 3. Local mass-transfer coefficient as a function of the axial position, all segments connected. Part (a): $Q = 2\ dm^3/min$. Part (b): $Q = 9\ dm^3/min$. Five independent measurements at each potential. Thin full line: mean value of the local mass-transfer coefficient at each segment. Error bars: standard deviation. Thick full line: global mass-transfer coefficient. Dashed line: global mass-transfer coefficient for an annular duct with axial flow according to Eqs. (3) or (4).

electrode length. However, in all cases it was possible to identify a potential region working the test reaction under limiting current conditions. The thin full lines in Fig. 3 join the mean values of the local mass-transfer coefficient at each segment, calculated from different cathodic potentials, and the error bars represent the standard deviation. Fig. 3, with all segments connected, corroborates the mass-transfer behaviour reported on Fig. 2. The decay of the mass-transfer performance along the reactor length is a consequence of that the swirling flow is dampened and also due to the fact that the concentration boundary layer starts developing after leaving the swirl generator at the reactor inlet.

The mass transfer coefficient in a smooth annular duct with axial developing flow and lateral ports for the inlet and outlet of the electrolyte is given by [23]:

$$\mathrm{Sh} = 1.029\mathrm{Re}^{0.55}\mathrm{Sc}^{1/3}\left(\frac{L}{d_e}\right)^{-0.472} \tag{3}$$

for $400 < \mathrm{Re} < 2000$ and

$$\mathrm{Sh} = 0.095\mathrm{Re}^{0.85}\mathrm{Sc}^{1/3}\left(\frac{L}{d_e}\right)^{-0.472} \tag{4}$$

for $3000 < \mathrm{Re} < 10{,}000$. Eqs. (3) and (4) are valid for $1100 < \mathrm{Sc} < 5200$ and $6.8 < L/d_e < 34.4$. Here, Sh, Re and Sc are the Sherwood, Reynolds and Schmidt numbers, respectively, defined as:

$$\mathrm{Sh} = \frac{k_m d_e}{D} \tag{5}$$

$$\mathrm{Re} = \frac{u_{av} d_e}{\nu} \tag{6}$$

and

$$\mathrm{Sc} = \frac{\nu}{D} \tag{7}$$

being d_e the equivalent diameter of the annulus (given by the difference between the outer and inner diameters), D the diffusion coefficient, L the annulus length, ν the kinematic viscosity and u_{av} the average fluid velocity in the annulus. In order to have a basis for evaluating the degree of mass-transfer enhancement, the mass-transfer coefficient

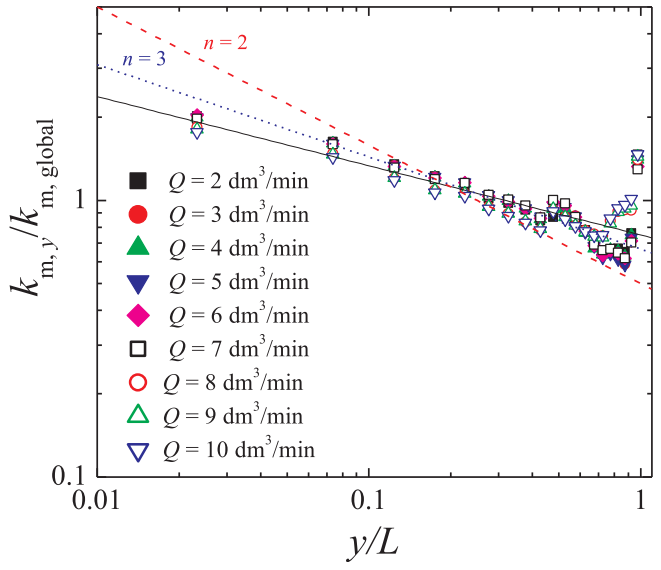

Fig. 4. Dimensionless ratio between the local and global mass-transfer coefficients as a function of the axial position for different values of volumetric flow rate. Single-phase flow. Full line: correlation according to Eq. (8) with $n = 4$. Dashed line: Eq. (8) with $n = 2$. Dotted line: Eq. (8) with $n = 3$.

according to Eq. (3) is represented as a dashed line in Fig. 3, part (a) and in part (b) based on Eq. (4). It can be seen that the global mass-transfer coefficient for helical flow, calculated by averaging all individual measurements with Eq. (2), is higher than that for an annular duct with developing axial flow, revealing the good performance of a device with swirling flow.

Fig. 4 shows the dimensionless ratio between local and global mass-transfer coefficients as a function of the axial position for the different inlet volumetric flow rates. The experimental results, neglecting the data at the reactor outlet, can be correlated by a relationship of the following type:

$$\frac{k_{m,y}}{k_{m,global}} = \frac{n-1}{n}\left(\frac{y}{L}\right)^{-1/n} \tag{8}$$

with $n = 4$, represented as full line in Fig. 4. Eq. (8) was deduced for a parallel-plate electrochemical reactor under laminar flow conditions with n between 2 and 3 depending on the development of the hydrodynamics [24], which are represented as dashed and dotted lines in Fig. 4, respectively. Therefore, Eq. (8) is also appropriate to represent the mass-transfer distribution in decaying swirling flow for regions away from the reactor outlet. Likewise, the uniformity of the current distribution can be characterised by the mean relative deviation, δ_{av}, which, taking into account Eq. (8), is given by [25]:

$$\delta_{av} = 2\frac{(n-1)^{n-1}}{n^n} \tag{9}$$

The distribution is more uniform as the mean relative deviation is smaller, representing an improvement in the reactor performance. δ_{av} results 0.21 for the present reactor with swirling flow. This low value gives a more uniform mass-transfer distribution in comparison with parallel-plate reactors under laminar flow conditions, which can also be recognised as an additional benefit of the swirling flow. The value of 4 for n agrees with that calculated from the empirical correlation of the local mass-transfer coefficient reported by Yapici et al. [13] for the outer wall in decaying annular swirling flow generated by an axial vane of 60°.

Fig. 5 reports on the global mass-transfer coefficient in dimensionless form as a function of the Reynolds number. The experimental data were correlated by the following expression, assuming that Sh is proportional to $Sc^{1/3}$:

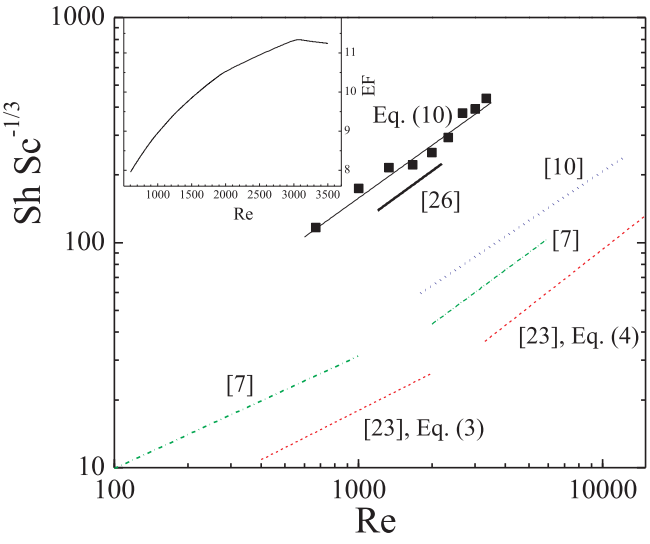

Fig. 5. Dimensionless correlation of the mass-transfer results for the single-phase flow. (■): experimental results. Full line: Eq. (10). Dashed lines: developing axial flow according to Eqs. (3) and (4) [23]. Dotted line: swirling flow according to [10]. Short dash-dotted line: swirling flow according to [7]. Thick full line: cylindrical part of a hydrocyclone [26]. Inset: Mass-transfer enhancement factor, EF, as a function of the Reynolds number.

$$Sh = 0.72Re^{0.78}Sc^{1/3} \tag{10}$$

Eq. (10) was determined for $600 < Re < 3500$ and $Sc = 2868$. Likewise, Eq. (10) is very close to the mass-transfer performance for the cylindrical part of a hydrocyclone [26]. A comparison with the results for an annular duct under developing flow conditions, Eqs. (3) and (4), is given. The inset presents the mass-transfer enhancement factor, EF, calculated as the ratio between Eq. (10) and Eqs. (3) or (4), in terms of the Reynolds number showing an important improvement of the mass-transfer performance by the swirling flow. Likewise, data from previous researches are included. The exponent of the Reynolds number in Eq. (10) is in accordance with previous studies. However, it is also observed that the present mass-transfer results are higher than the previous one. This can be attributed to two reasons: (i) the measurements were made at the outer electrode, that is more active than the inner part [13,14], with a single tangential entry causing a higher swirl intensity [11] and (ii) the abrupt expansion at the reactor inlet produces a recirculation zone just downstream of the entrance which interferes with the swirling flow enhancing the mass-transfer conditions. Legentilhomme and Legrand [8] reported that the mass-transfer in expansion swirl flow is greater than in pure swirl flow by a factor ranging from 1 to 1.8.

3.2. Mass-transfer studies in a two-phase (gas-liquid) system

Fig. 6 reports on typical mass-transfer distributions for single phase and two-phase flow, where a similar behaviour is observed in both cases. Fig. 7 compares the global mass-transfer coefficients in absence and presence of the gas phase. It can be stated that the gas phase presents a scarce influence on the mass-transfer conditions showing that the forced convection produced by the swirling flow is dominant in comparison with that of the gas phase. Only it is detected a small enhancement at low volumetric flow rates of the solution phase but at higher values the mass-transfer performance of the equipment slightly decreases. This is probably due to the fact that the presence of the gas phase disturbs the helical flow lowering the effect of the forced convection. Likewise, the dimensionless ratio between local and global mass-transfer coefficients as a function of the axial position in the presence of the gas phase yields a plot similar to Fig. 4. The results agree with Eq. (8) but with n ranging from 3.2 to 3.7, giving a mass-transfer distribution slightly less uniform in comparison with that of the

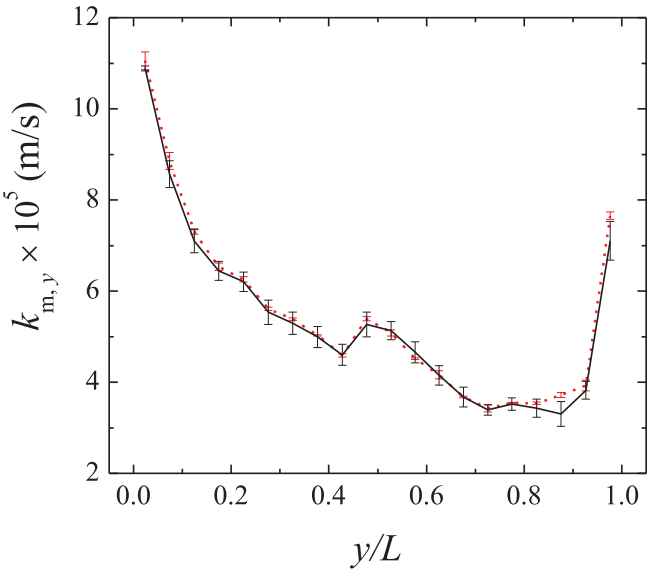

Fig. 6. Local mass-transfer coefficient as a function of the axial position, all segments connected. $Q = 6\,dm^3/min$. $Q_g = 2\,dm^3/min$ with inner feed. Full line: single phase flow. Dashed line: two-phase flow. Error bars: standard deviation for measurements at different cathodic potentials.

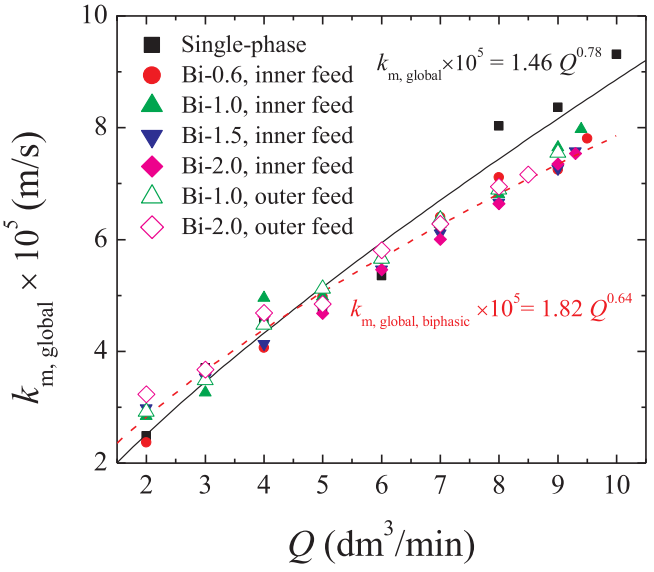

Fig. 7. Comparison of the global mass-transfer coefficients for the single-phase and two-phase flow. The numbers gives the gas volumetric flow rate for the biphasic system, Bi, in dm^3/min.

single phase case. The scarce influence of the gas feeder type, inner or outer feed, on the mass-transfer behaviour can be explained taking into account that due to the lower density of the gas and centripetal action, the gas phase immediately after the inlet moves toward the centre of the reactor, giving a similar hydrodynamics for the gas-liquid flow in both feed strategies. This explanation was corroborated by flow visualization experiments carried out by injecting nitrogen gas or air in equipments with decaying swirling flow [15,27]. The correlation equations are also reported on Fig. 7 and Eq. (11) gives the dimensionless relationship for the mass-transfer in presence of the gas phase:

$$Sh = 2.13 Re^{0.64} Sc^{1/3} \quad (11)$$

Eq. (11) is valid for $600 < Re < 3500$, $19 < Re_{gas} < 65$ and $Sc = 2868$. The exponent in the Reynolds number in Eq. (11) is lower than under single phase, Eq. (10), showing a minor influence of the volumetric flow rate on the global mass-transfer coefficient because the presence of the gas phase alters the swirling flow conditions.

4. Conclusions

The experimental study of mass-transfer at the external electrode of an electrochemical reactor with decaying swirling flow produced by tangential inlet and outlet of the electrolyte solution yields high values of the mass-transfer enhancement factor, from 8 to 11, increasing with Reynolds number. The improvement in the mass-transfer conditions can be attributed to the intensive convection flow at the surface of the external electrode produced by the swirling flow, which is complemented by a hydrodynamic perturbation due to the expansion at the reactor entrance as a consequence of that the diameter in the tangential inlet port is smaller than the interelectrode gap. The experimental results are well correlated by a dimensionless equation involving the Sherwood and Reynolds numbers, in terms of the equivalent diameter of the annulus as characteristic length. Thus, the good mass-transfer behaviour of the swirling flow in comparison with other strategies was corroborated. The introduction of a gas phase together with the electrolyte solution presents scarce influence on the mass-transfer performance of the equipment, showing swirling flow as a promising alternative to be examined for biphasic electrochemical reactors.

Acknowledgements

This work was supported by the Agencia Nacional de Promoción Científica y Tecnológica (ANPCyT), Consejo Nacional de Investigaciones Científicas y Técnicas (CONICET) and Universidad Nacional del Litoral (UNL) of Argentina.

References

[1] N.J. Cedrone, A silver-recovery apparatus for operation at high current densities, J. SMPTE 67 (1958) 172–174.
[2] F.C. Walsh, G. Wilson, The electrolytic removal of gold from spent electroplating liquors, Trans. Inst. Met. Finish. 64 (1986) 55–62.
[3] S. Wang, Recovering copper using a combination of electrolytic cells, JOM 54 (2002) 51–54.
[4] S. Wang, Novel electrowinning technologies: the treatment and recovery of metals from liquid effluents, JOM 60 (2008) 41–45.
[5] R. Parmar, S.K. Majumder, Microbubble generation and microbubble-aided transport process intensification—a state-of-the-art report, Chem. Eng. Process. 64 (2013) 79–97.
[6] E. Shoukry, L.W. Shemilt, Mass transfer enhancement in swirling annular pipe flow, Ind. Eng. Chem. Process Des. Dev. 24 (1985) 53–56.
[7] P. Legentilhomme, J. Legrand, Overall mass transfer in swirling decaying flow in annular electrochemical cells, J. Appl. Electrochem. 20 (1990) 216–222.
[8] P. Legentilhomme, J. Legrand, The effects of inlet conditions on mass transfer in annular swirling decaying flow, Int. J. Heat Mass Transfer 34 (1991) 1281–1291.
[9] P. Legentilhomme, H. Aouabed, J. Legrand, Developing mass transfer for annular swirling decaying flow induced by means of a tangential inlet, Chem. Eng. J. 52 (1993) 137–147.
[10] M.S. de Sa, L.W. Shemilt, I.V. Soegiarto, Mass transfer in the entrance region for axial and swirling annular flow, Can. J. Chem. Eng. 69 (1991) 294–299.
[11] S. Yapici, M.A. Patrick, A.A. Wragg, Hydrodynamics and mass transfer in decaying annular swirl flow, Int. Comm. Heat Mass Transfer 21 (1994) 41–51.
[12] S. Yapici, M.A. Patrick, A.A. Wragg, Electrochemical study of mass transfer in decaying annular swirl flow. Part 1: axial distribution of local mass transfer coefficients, J. Appl. Electrochem. 24 (1994) 685–693.
[13] S. Yapici, M.A. Patrick, A.A. Wragg, Electrochemical study of mass transfer in decaying annular swirl flow Part II: correlation of mass transfer data, J. Appl. Electrochem. 25 (1995) 15–22.
[14] G. Lefèbvre, S.R.F. Neto, H. Aouabed, P. Legentilhomme, J. Legrand, Transfert de matière et chute de pression lors d'un écoulement tourbillonnaire annulaire non-entretenu induit par une entrée tangentielle, Can. J. Chem. Eng. 76 (1998) 1039–1050.
[15] S. Yapici, G. Yazici, C. Özmetin, H. Erşahan, Ö. Çomakli, Mass transfer to local electrodes at wall and wall friction factor in decaying turbulent swirl flow, Int. J. Heat Mass Transfer 40 (1997) 2775–2783.
[16] O. Wein, K. Wichterle, Theory of segmented electrodiffusion probes: the effect of insulating insertions, Collect. Czech. Chem. Commun. 54 (1989) 3198–3212.
[17] A.N. Colli, J.M. Bisang, The effect of a perpendicular and cumulative inlet flow on the mass-transfer distribution in parallel-plate electrochemical reactors,

Electrochim. Acta 137 (2014) 758–766.
[18] A.N. Colli, J.M. Bisang, A CFD study with analytical and experimental validation of laminar and turbulent mass-transfer in electrochemical reactors, J. Electrochem. Soc. 165 (2018) E81–E88.
[19] H. Brown, B.B. Knapp, Nickel, in: F.A. Lowenheim (Ed.), Modern Electroplating, John Wiley & Sons, New York, 1974, pp. 287–341.
[20] R. Battino, T.R. Rettich, T. Tominaga, The solubility of oxygen and ozone in liquids, J. Phys. Chem. Ref. Data 12 (1983) 163–178.
[21] A.N. Colli, J.M. Bisang, Comparison of the performance of flow-by three-dimensional cylindrical electrochemical reactors with inner or outer counter electrode under limiting current conditions, Electrochim. Acta 154 (2015) 468–475.
[22] J.R. Selman, C.W. Tobias, Mass-transfer measurements by the limiting-current technique, in: T.B. Drew, G.R. Cokelet, J.W. Hoopes, T. Vermeulen (Eds.), Advances in Chemical Engineering, Academic Press, New York, 1978, pp. 211–318.
[23] A.A. Mobarak, H.A. Farag, G.H. Sedahmed, Mass transfer in smooth and rough annular ducts under developing flow conditions, J. Appl. Electrochem. 27 (1997) 201–207.
[24] A.N. Colli, J.M. Bisang, Validation of theory with experiments for local mass transfer at parallel plate electrodes under laminar flow conditions, J. Electrochem. Soc. 160 (2013) E5–E11.
[25] A.N. Colli, J.M. Bisang, Combination of cumulative and convergent flows as a means to improve the uniformity of tertiary current distribution in parallel-plate electrochemical reactors, J. Electrochem. Soc. 164 (2017) E42–E47.
[26] L.C. Resio, O. González Pérez, J.M. Bisang, Mass-transfer study and copper ions removal using a modified hydrocyclone as electrochemical reactor, J. Electrochem. Soc. 164 (2017) E529–E535.
[27] K.S. Jun, S.C. Jain, Oxygen transfer in bubbly turbulent shear flow, J. Hydraul. Eng. 119 (1993) 21–36.